Urban aerosol chemistry at a land-water transition site during summer – Part 2: Aerosol pH and liquid water content

Michael A. Battaglia, Jr.[1,a], Nicholas Balasus[1], Katherine Ball[1], Vanessa Caicedo[2], Ruben Delgado[2], Annmarie G. Carlton[3] , and Christopher J. Hennigan[1*]

[1]Department of Chemical, Biochemical, and Environmental Engineering, University of Maryland, Baltimore County

[2]Joint Center for Earth Systems Technology, University of Maryland, Baltimore County

[3]Department of Chemistry, University of California, Irvine

[a]Current affiliation: School of Earth and Atmospheric Sciences, Georgia Institute of Technology

Correspondence: C. J. Hennigan (hennigan@umbc.edu)

1 **Abstract**
2
3   Particle acidity (aerosol pH) is an important driver of atmospheric chemical processes

4 and the resulting effects on human and environmental health. Understanding the factors that

5 control aerosol pH is critical when enacting control strategies targeting specific outcomes. This

6 study characterizes aerosol pH at a land-water transition site near Baltimore, MD during summer

7 2018 as part of the second Ozone Water-Land Environmental Transition Study (OWLETS-2)

8 field campaign. Inorganic fine mode aerosol composition, gas-phase NH_3 measurements, and all

9 relevant meteorological parameters were used to characterize the effects of temperature, aerosol

10 liquid water (ALW), and composition on predictions of aerosol pH. Temperature, the factor

11 linked to the control of NH_3 partitioning, was found to have the most significant effect on aerosol

12 pH during OWLETS-2. Overall, pH varied with temperature at a rate of -0.047 K^{-1} across all

13 observations, though the sensitivity was -0.085 K^{-1} for temperatures > 293 K. ALW had a minor

14   effect on pH, except at the lowest ALW levels (< 1 µg m^{-3}) which caused a significant increase

15   in aerosol acidity (decrease in pH). Aerosol pH was generally insensitive to composition (SO_4^{2-},

16   SO_4^{2-}:NH_4^+, Tot-NH_3 = NH_3 + NH_4^+), consistent with recent studies in other locations. In a

17   companion paper, the sources of episodic NH_3 events (95th percentile concentrations, $NH_3 > 7.96$

18   µg m^{-3}) during the study are analyzed; aerosol pH was higher by only ~0.1-0.2 pH units during

19   these events compared to the study mean. A case study was analyzed to characterize the

20   response of aerosol pH to nonvolatile cations (NVCs) during a period strongly influenced by

21   primary Chesapeake Bay emissions. Depending on the method used, aerosol pH was estimated

22   to be either weakly (~0.1 pH unit change based on NH_3 partitioning calculation) or strongly

23   (~1.4 pH unit change based on ISORROPIA thermodynamic model predictions) affected by

24   NVCs. The case study suggests a strong pH gradient with size during the event and underscores

25   the need to evaluate assumptions of aerosol mixing state applied to pH calculations. Unique

26   features of this study, including the urban land-water transition site and the strong influence of

27   NH_3 emissions from both agricultural and industrial sources, add to the understanding of aerosol

28   pH and its controlling factors in diverse environments.

1 Introduction

The acidity, or pH, of atmospheric aerosols affects the chemical and physical properties of airborne particles, and thus, their impacts on climate and health (Pye et al., 2020). The gas-particle partitioning of semi-volatile acidic and basic compounds – notably NH_3, HNO_3, HCl, and organic acids – depends in part on aerosol pH, which directly affects the particulate matter (PM) mass concentration (Nenes et al., 2020). The solubility of many particulate components is pH-dependent, including metals and nutrients, with implications for particle toxicity and nutrient deposition to ecosystems (Fang et al., 2017; Kanakidou et al., 2016). The optical properties of light-absorbing organic compounds, known as brown carbon, can exhibit a strong pH-dependence, which directly affects their climate impacts (Phillips et al., 2017). Given the importance of aerosol pH for atmospheric processes and the limitation in estimating acidity with proxies (e.g., ion balances), there has been increased effort in recent years to identify the factors that affect pH and to characterize temporal and spatial variations in the atmosphere (Hennigan et al., 2015).

Globally, aerosol pH is often quite acidic due to the ubiquity and abundance of strong acids like H_2SO_4, HNO_3, and HCl (Pye et al., 2020). Ammonia (NH_3) is unique among species that affect pH because it is the most abundant basic compound in the atmosphere. NH_3 partitioning is controlled by the concentration of strong acids and by the ambient temperature and relative humidity, hence, the dependence of pH on both composition and meteorology (Zheng et al., 2020). This explains why NH_3 can exist partially in the gas phase even when the aerosol pH is highly acidic (Weber et al., 2016). Due to its abundance and semi-volatile properties, NH_3 was identified as the most important buffering agent in aerosols across locations with diverse emissions, composition, and climatology (Zheng et al., 2020). In single-phase

3

53   aqueous particles, organic compounds have a minor effect on pH (Battaglia Jr et al., 2019),

54   though this is not the case for particles that have undergone liquid-liquid phase separation (Pye et

55   al., 2018). Non-volatile cations (NVC) typically contribute a minor fraction of PM mass but can

56   be critical for accurate predictions of pH, especially if NVC concentrations are overestimated

57   (Vasilakos et al., 2018). Globally, NVC are most important in regions heavily impacted by dust

58   emissions (Pye et al., 2020), but have minor effects on pH in other regions (Tao and Murphy,

59   2019; Zheng et al., 2020).

60   Aerosol pH is also strongly affected by meteorological factors. Equilibrium constants,

61   including those that determine the gas-particle partitioning and aqueous dissociation of semi-

62   volatile acids and bases, are temperature dependent. Temperature is a dominant factor driving

63   variability in the seasonal and diurnal cycling of pH (Guo et al., 2015; Tao and Murphy, 2019).

64   Temperature gradients, as occur in and around urban areas, can also drive large differences in

65   pH, even if the composition is uniform over the same scales (Battaglia et al., 2017). Relative

66   humidity (RH) regulates aerosol liquid water content (ALWC), which affects the partitioning of

67   soluble gases and aqueous phase solute concentrations. ALWC may be the most important

68   factor responsible for large pH differences observed between the southeast US (pH ~0.5-1.0) and

69   the heavily polluted North China Plain (pH ~4-5), the two regions where pH has been most

70   extensively studied to-date (Zheng et al., 2020). These effects can be complex, or even partially

71   offset. For example, an increase in temperature reduces pH owing to the shift in NH_3

72   partitioning towards the gas phase, but NH_3 emissions increase with temperature as well,

73   producing an increase in pH and partially offsetting the pH changes due to temperature (Tao,

74   2020). More research is needed to better understand how all these factors together affect pH, and

75   how this changes geographically and temporally.

76   In this study aerosol pH was characterized during the summertime (June 4 to July 5,

77   2018) at a land-water transition site near a large urban area (Baltimore, MD) as part of the

78   OWLETS-2 (second Ozone Water-Land Environmental Transition Study) field campaign. This

79   site is unique because meteorological phenomena, such as the bay breeze, affect pollution

80   dispersion and recirculation (Loughner et al., 2014). Baltimore is impacted by different regional

81   emission sources, as it is located in the populous and heavily trafficked I-95 corridor, and

82   downwind of the Ohio River Valley (He et al., 2013), and relatively close to regional agricultural

83   operations that emit large amounts of NH_3 (Pinder et al., 2006). In the companion investigation,

84   the local sources of NH_3 during the OWLETS-2 study were examined, including an analysis of

85   transient events with unexpectedly high NH_3 concentrations (Balasus et al., 2021). In this study,

86   the effects of the observed NH_3 concentrations (including transient concentrations of

87   unexpectedly high values), in combination with the unique meteorological phenomena associated

88   with the land-water transition, on ALW and aerosol pH were investigated.

89

90   **2 Methods**

91   The OWLETS-2 study was conducted to characterize effects of meteorological

92   phenomena associated with the land-water transition on summertime air quality in Baltimore.

93   Hart-Miller Island (HMI, coordinates 39.2421°, -76.3627°), a site located on the Chesapeake Bay

94   ~10 km east of downtown Baltimore, hosted many of the ground-based measurements during the

95   study (Fig. S1). Semi-continuous measurements of aerosol inorganic chemical composition and

96   gas-phase NH_3 were conducted at HMI. The measurement details are provided in the companion

97   paper (Balasus et al., 2021). Briefly, the water-soluble ionic components of $PM_{2.5}$ were

98   measured with a Particle-into-Liquid Sampler coupled to a dual Ion Chromatograph (PILS-IC,

99 Metrohm) operated according to Valerino et al. (2017). NH₃ was measured with an AiRRmonia

100 Analyzer (RR Mechatronics) (Norman et al., 2009). Meteorological parameters were measured

101 with a Vaisala MAWS201 Met Station at 1-minute resolution.

102   The 5-minute NH₃ measurements and 1-minute meteorological measurements were

103 averaged to the 20-mintue sampling time of the PILS-IC. Aerosol pH for each 20-min sample

104 was calculated according to Zheng et al. (2020). This method uses the relevant temperature-

105 dependent equilibrium constants and the measured concentrations of NH₃ and [NH₄⁺] to

106 calculate pH. The method of Zheng et al. (2020) is based upon a similar approach in prior

107 studies (Hennigan et al., 2015; Keene et al., 2004), with minor differences possibly due to

108 equilibrium constant values and/or the concentration basis (molality vs. molarity). Indeed, very

109 close agreement was observed (slope = 0.967, R^2 = 0.977, n = 872, Fig. S2) in calculated pH

110 between the methods of Zheng et al. (2020) and Hennigan et al. (2015). The aqueous phase

111 NH_4^+ concentration is derived from the mass concentration of NH_4^+ from the PILS-IC and the

112 ALWC. The ISORROPIA-II thermodynamic equilibrium model was used to calculate ALW

113 using the PILS-IC, NH₃, and meteorological data as inputs (Fountoukis and Nenes, 2007). The

114 model was run in forward mode (NH₃ and aerosol NH_4^+ were input at total NH₃) using the

115 metastable assumption according to the recommendation of Guo et al. (2015).

116   Although ISORROPIA can provide pH, the methods of Zheng et al. (2020) and Tao et al.

117 (2020) were used for pH calculations:

118
$$pH = pK_{a,NH_3}^* + log_{10} \frac{[NH_3(aq)] + [NH_3(g)]}{[NH_4^+(aq)]} \tag{1}$$

119
$$[NH_3(g)] = \frac{p_{NH_3}\rho_w}{RT \, AWC} \tag{2}$$

120
$$K_{a,NH_3}^* = \frac{[H^+(aq)]([NH_3(aq)] + [NH_3(g)])}{[NH_4^+(aq)]} = K_{a,NH_3}\left(1 + \frac{\rho_w}{H_{NH_3}RT \, AWC}\right) \tag{3}$$

121   where in Equation 1, $[NH_3(aq)]$ is the molality of NH_3 in solution (mol kg^{-1}, calculated by

122   multiplying H_{NH_3} and p_{NH_3}), $[NH_3(g)]$ is the equivalent molality of gaseous NH_3 in solution

123   (mol kg^{-1}, given by Equation 2), and $[NH_4^+(aq)]$ is the molality of NH_4^+ in solution (mol kg^{-1}).

124   Equation 2 calculates $[NH_3(g)]$, where p_{NH_3} is the partial pressure of NH_3 (atm), ρ_w is the

125   density of water (µg m^{-3}), R is the gas constant (atm L mol^{-1} K^{-1}), T is temperature (K), and

126   AWC is aerosol water content (µg m^{-3} air). Equation 3 calculates the last unknown term in

127   Equation 1, which is K_{a,NH_3}^*, the effective dissociation constant (where H_{NH_3} is the Henry's law

128   constant of NH_3 in mol kg^{-1} atm^{-1}).

129   Direct measurements of aerosol pH are not available to test model predictions so the

130   partitioning of semi-volatile species that depend on pH, most commonly NH_3/NH_4^+ and

131   HNO_3/NO_3^-, is a key metric used to evaluate model performance (Pye et al., 2020).

132   ISORROPIA is used extensively for predictions of pH; however, in this study the measured and

133   ISORROPIA-predicted values of NH_3 partitioning (ε_{NH3} = NH_3/(NH_3 + NH_4^+)) did not agree well

134   (Fig. S3). There were systematic differences in pH between the two methods (mean pH

135   difference = 0.6 pH units), and they were not correlated (R^2 = 0.097, not shown). The source of

136   the discrepancy in NH_3 partitioning (ISORROPIA modeled versus measurement-calculated) is

137   unknown, though it is not likely the result of an incorrect assumption of equilibrium (see the SI

138   and the companion paper Balasus et al. (2021) for more details).

139

140   **3 Results and Discussion**

141   **3.1 Meteorological effect on pH**

142   As in many cities, the urban heat island effect in Baltimore evolves throughout the day,

143   with urban-rural temperature and RH gradients peaking at night (Battaglia et al., 2017).

144   Meteorological conditions at HMI demonstrate unique features associated with the land-water

145   transition. At night, the average temperature observed at HMI was close to conditions observed

146   in downtown Baltimore but transitioned to match the conditions at a nearby rural site during the

147   day (Fig. 1a). Overall, the range in average hourly temperatures at HMI was lower (4.3 °C; 22.5

148   – 26.8 °C) than the averages observed at either the downtown site (range 6.2 °C; 22.8 – 29.0 °C)

149   or the rural site (range 8.8 °C; 17.5 – 26.3 °C). Likewise, the average hourly RH profile at HMI

150   had a significantly smaller range (13.7%; 61.7 – 75.4%) than the RH profiles at the downtown

151   (range 22.1%; 53.2 – 75.3%) or rural sites (range 30.3%; 55.9 – 86.2%) (Fig. 1b). The

152   differences shown in Fig. 1 were due to the proximity of HMI to the Chesapeake Bay. This has

153   strong implications for aerosol pH, which will be discussed in detail below.

154   Due to the meteorological conditions discussed above, the diurnal profile of ALWC at

155   HMI was unique (Fig. 2a). Typical profiles of ALWC in the eastern US closely follow RH, with

156   minima in the afternoon and maxima at night or in the pre-dawn morning hours (Guo et al.,

157   2015; Battaglia et al., 2017). During OWLETS-2, ALWC did not show a distinct diurnal profile

158   that was correlated with RH. Instead, the highest median ALWC at HMI occurred between

159   12:00 – 14:00, (local time, LT; during the study this is UTC-4) (Fig. 2a). This daily peak in

160   ALWC coincided with a pronounced enhancement in aerosol NO_3^-, which is discussed in the

161   companion paper (Balasus et al., 2021). The partitioning of NH_3, ε_{NH3}, also showed a diurnal

162   profile that was unexpected (Fig. 2b). Due to the strong temperature dependence of vapor

163   pressure and equilibrium constants, NH_3 partitioning typically shifts towards the gas-phase

164   during the daytime (ε_{NH3} increases) and shifts towards the aerosol phase at night (ε_{NH3} decreases)

165   (Guo et al., 2017). The increase in gas-phase NH_3 emissions with increasing temperature can

166   also contribute to an elevated ε_{NH3} during the daytime. The diurnal profile of ε_{NH3} observed at

167   HMI did not follow temperature, as the median ε_{NH3} peaked during the 06:00 – 08:00 LT, and

168   decreased slightly into the afternoon (Fig. 2b). This shows a shift of NH_3 partitioning towards

169   the condensed phase as daily temperatures peaked. This was allowed by the ALWC remaining

170   steady throughout the afternoon. Overall, the median ε_{NH3} value for the entire OWLETS-2 study

171   was 0.915, showing NH_3 partitioning was shifted towards the gas-phase.

172   The diurnal profile of aerosol pH computed using the method of Zheng et al. (2020)

173   followed a qualitatively similar pattern to prior studies (Battaglia et al. 2017), with maxima in

174   the early morning and minima in the afternoon; however, there was a much smaller amplitude in

175   the median hourly pH values (Fig. 3). The highest median pH value (1.97) was observed

176   between 07:00 – 08:00 LT, while the lowest median pH (1.50) was observed between 16:00 –

177   17:00 LT. For the entire study, there was only a ~1 pH unit difference between the 10th and 90th

178   percentile values (1.39 and 2.36, respectively). The relatively muted diurnal profile of aerosol

179   pH was due to the unique meteorology that resembled a nearby urban site at night and

180   transitioned to match the nearby rural site during the day. The companion paper shows the

181   diurnal profiles of aerosol inorganic composition (Balasus et al., 2021). Figures 2 and 3 are

182   consistent with recent studies that demonstrate the high sensitivity of pH to meteorological

183   factors (Battaglia et al., 2017; Tao and Murphy, 2019; Zheng et al., 2020).   It is interesting to

184   note that the ISORROPIA predictions of aerosol pH yield a distinctly different diurnal profile

185   than the pH predicted by NH_3 partitioning (Fig. S4). The difference in pH between the two

186   methods peaked in the afternoon between 12:00 – 14:00 LT, when particles were most acidic,

187   and was a minimum in the early morning when pH was highest (Fig. S4). The reason for these

188   discrepancies are explored in the discussion below.

189   Results suggest that pH was most sensitive to temperature changes at HMI during

190   OWLETS-2 (Fig. 4a). Across the full temperature range, the observed pH sensitivity to

191   temperature was -0.047 K^{-1}. A recent study contrasting pH in the southeast US and the North

192   China Plain found that temperature affects pH linearly at a rate of approximately -0.055 K^{-1}

193   (Zheng et al., 2020). A separate study from a Canadian observational network found that the

194   pH-temperature dependence is not linear, but changes with temperature (Tao and Murphy, 2019;

195   Tao, 2020). Over the range of conditions observed during OWLETS-2, Tao (2020) computed a

196   pH sensitivity to temperature of approximately -0.045 K^{-1} to -0.055 K^{-1}. In a previous study, the

197   pH sensitivity to temperature in Baltimore was -0.048 K^{-1}, though this was calculated for

198   conditions of constant atmospheric composition (Battaglia et al., 2017). While present results

199   share consistencies with these studies, the results in Fig. 4a suggest important differences, as

200   well. An increase in pH was observed with increasing temperature for conditions below 293 K

201   (n=156). In the companion paper, NH_3 concentrations dramatically increased with temperature <

202   293 K but exhibited a much weaker dependence on temperature for conditions > 293 K (Balasus

203   et al., 2021). Under the warmer conditions, the pH relationship with temperature was linear

204   during OWLETS-2, with a sensitivity of -0.085 K^{-1} (Fig. 4a). The results in Fig. 4a are

205   consistent with Tao (2020), as they demonstrate the offsetting responses of pH to temperature

206   through effects on NH_3 emissions and partitioning.

207   These results contribute to the growing body of work demonstrating the importance of

208   temperature to aerosol pH. Collectively, these studies suggest that the sensitivity of pH to

209   temperature is constrained between -0.045 K^{-1} and -0.085 K^{-1}, although the present results

210   illustrate circumstances where a positive relationship between temperature and pH can exist, as

211   well. It is notable that similar $\Delta pH/\Delta T$ values are observed across a range of locations and for

212   variable data sets that include monthly averages of long-term observations (Tao and Murphy,

213   2019) and 20-min measurements made over a period of weeks (presented here).

214   Aerosol pH was not strongly affected by ALWC over the range of conditions observed

215   during OWLETS-2, except at ALWC below 1 μg m^{-3} (Fig. 4b). At the lowest ALWC levels, the

216   increase in pH occurs because of the diluting effect of water, however, at ALWC above 1 μg m^{-3},

217   other factors appear to be more important (e.g., temperature). ALWC was recently identified as

218   the most significant contributor to regional pH differences (Zheng et al., 2020). In that study, the

219   pH-ALWC relationship was highly non-linear, with the greatest sensitivity calculated at ALWC

220   at levels < 25 μg m^{-3}, conditions corresponding to all the OWLETS-2 observations. Tao (2020)

221   found that pH is extremely sensitive to RH, presumed to be a surrogate for ALWC, when RH

222   was < 20% or RH > 80%; however, pH was quite insensitive to RH variations in the region of

223   20% < RH < 80%. Approximately 25% (208 out of 875) of RH values during OWLETS-2 were

224   above 80%, yet no increase in pH was observed at the highest ALWC, suggesting that other

225   factors were offsetting the diluting effect of water as ALWC increased. It is interesting to note

226   that ISORROPIA predicts a stronger effect of ALWC on pH, with the diluting effect apparent as

227   pH increases with increasing ALWC (Fig. 4b).

228   The result shown in Fig. 4b is somewhat surprising because NH_3 partitioning was quite

229   sensitive to ALWC (Fig. 5); the relatively invariant aerosol pH is unexpected given the increase

230   in NH_3 uptake in the presence of ALW. NH_3 partitioning shifted towards the condensed phase

231   (ε_{NH3} decreased) at increasing ALWC, consistent with the results of Nenes et al. (2020). ε_{NH3}

232   was more sensitive to ALWC than it was to either temp or RH (Fig. S6). This result shows the

233   importance that ALWC can have on $PM_{2.5}$ mass concentrations, as water serves as an important

234   medium enhancing the condensation of organic and inorganic water-soluble species (Carlton et

235 al., 2018; El-Sayed et al., 2016). Fig. 5 demonstrates the importance of ALWC in changing the

236 dry deposition of reactive nitrogen species. Nenes et al. (2021) predicts that NH_3 and HNO_3 dry

237 deposition rates will both be high under the conditions observed during OWLETS-2 (i.e., ALWC

238 < 10 µg m^{-3} and pH ~ 1.5). This is also consistent with a modeling study showing increased dry

239 deposition of reactive nitrogen in coastal regions, including the OWLETS-2 study domain

240 (Loughner et al., 2016).

241

242 **3.2 Composition Effects on Aerosol pH**

243   In contrast to meteorological factors, aerosol composition did not have a major effect on

244 pH variability during OWLETS-2. Consistent with prior studies, neither the sulfate

245 concentration nor the NH_4^+:SO_4^{2-} molar ratio contributed significantly to pH variability (Weber

246 et al., 2016; Hennigan et al., 2015). Fig. 4c shows that pH was also relatively insensitive to the

247 Tot-NH_3 concentration, in agreement with the results from other locations (Zheng et al., 2020;

248 Tao, 2020; Weber et al., 2016). While the predictions of ISORROPIA generally did not capture

249 the trends between pH and the meteorological factors, it is interesting to note that ISORROPIA

250 predicts that pH is relatively insensitive to Tot-NH_3, as well, except at the highest concentrations

251 (Fig. S5).

252   Composition and concentration differences between HMI and the urban and rural sites

253 are analyzed in more detail in the companion paper (Balasus et al., 2021). In the companion

254 paper, episodic NH_3 events that derived from dairy, poultry, and industrial sources were

255 characterized (Balasus et al., 2021). For the events with complete aerosol composition and

256 meteorology data (8 out of 11 NH_3 events total), the average and medial aerosol pH values (2.00

257 and 1.96, respectively) were only moderately higher than the study average and median pH

258   values (1.85 and 1.83, respectively); this difference is not statistically significant at the 95%

259   confidence interval. This includes an aerosol pH of 1.92 at the peak NH_3 concentration observed

260   during the entire study (19.3 μg m^{-3}), an event influenced by industrial emissions near downtown

261   Baltimore (Balasus et al., 2021). Together, the results suggest that pH may be more affected by

262   the proximity of the HMI site to the Chesapeake Bay than it was to regional agricultural NH_3

263   emissions, or to episodic NH_3 events from local industrial sources.

264

265   **3.3 Case Study: Effect of NVCs on pH**

266   NVCs affect thermodynamic predictions of NH_3 partitioning and thus, pH (Guo et al.,

267   2018; Vasilakos et al., 2018). Seawater is alkaline and primary marine emissions contain high

268   concentrations of NVCs (O'Dowd and De Leeuw, 2007). Marine aerosols rapidly acidify,

269   typically in seconds or minutes, though the timescale depends upon particle size (Angle et al.,

270   2021; Pszenny et al., 2004). Studies have examined the acidity of sea spray aerosols and their

271   evolution but none, to the authors' knowledge, have done so in a polluted urban environment.

272   The OWLETS-2 study offered a unique opportunity to analyze the pH of primary marine

273   particles emitted within several km of a large urban area. The Chesapeake Bay is brackish, with

274   increasing salinity moving down the bay towards the Atlantic Ocean (Pritchard, 1952). Near the

275   OWLETS-2 measurement site at HMI, salinity is variable but average conditions are ~5 g kg^{-1}

276   (www.chesapeakebay.net, last accessed 20-November 2020). This is about a factor of seven

277   lower than typical seawater, but shows the potential for primary emissions to contribute salts that

278   could impact aerosol pH at HMI.

279   Elevated concentrations of Na^+ and Cl^- in $PM_{2.5}$ were infrequently observed during

280   OWLETS-2, with one notable 36-hour period showing evidence of primary marine impact. Na^+

281   and Cl⁻ were well-correlated (R^2 = 0.78) from 11-June to 13-June, a period that coincided with

282   the highest concentrations of both species (Fig. 6 and Fig. 7). It is noteworthy that wind speeds

283   were not elevated during this time (average winds = 3.1 m s⁻¹ compared to campaign-average

284   wind speeds of 2.9 m s⁻¹); longer-term measurements would be needed to characterize factors

285   driving the primary bay emissions. During this event, the pH calculation using NH_3 partitioning

286   suggests that the primary marine emissions had a minimal effect on aerosol pH. The average pH

287   during this period was 1.98, which was only slightly higher than the average for the entire study

288   (1.85). Further, as the total Na^+ + Cl⁻ concentration increased by more than an order of

289   magnitude, from 0.05 μg m⁻³ around 18:00 LT on 11 June to 0.9 μg m⁻³ at 09:00 LT on 12 June,

290   the pH only increased by 0.1 pH unit during the same period (Fig. 6). Gas-phase NH_3 data were

291   not available for the entire NaCl event, so pH calculations were limited to the first ~20 hours.

292   The pH predictions from ISORROPIA during this period display a more significant effect

293   on aerosol pH. The average pH predicted by ISORROPIA is 3.08, which is 0.7 pH units higher

294   than the study average from ISORROPIA. Further, while the pH calculated using NH_3

295   partitioning is insensitive to Na^+ and Cl⁻, ISORROPIA predicts a rise of 1.4 pH units as Na^+ and

296   Cl⁻ increase (Figure 6). The NH_3 partitioning predicted by ISORROPIA deviates from the

297   observations during this event (r = -0.19, Fig. S7). The most likely explanation for this behavior

298   is different chemical compositions of the coarse- and fine-mode particles. Fresh marine

299   emissions acidify quickly, and evidence was found for chemical processing of NaCl. HNO_3

300   displacement of HCl is a well-known phenomenon in sea salt particles (Brimblecombe and

301   Clegg, 1988). Chloride:sodium ratios slightly above unity were observed when aerosol nitrate

302   concentrations were low, and below unity when nitrate concentrations were elevated (Fig. 7).

303   Nitrate formation, including HNO_3 uptake to sea salt, is highly sensitive to pH (Kakavas et al.,

14

304   2021; Vasilakos et al., 2018). Nitrate (along with Na^+ and Cl^-) are direct inputs to ISORROPIA,

305   suggesting that the pH trend in Fig. 6 is due to the increased influence of coarse-mode particles.

306   The PILS inlet was equipped with a 2.5 μm cut-point cyclone (URG-2000-30-EH, URG Corp.),

307   which allows some penetration of particles with d_p < 4.5 μm

308   (http://www.urgcorp.com/products/inlets/teflon-coated-aluminum-cyclones/urg-2000-30eh, last

309   accessed 29 January 2021). Likewise, primary sea salt emissions often exhibit a size distribution

310   tail that extends below 2.5 μm (Feng et al., 2017).

311   The above analysis identifies limitations computing aerosol pH with both approaches and

312   highlights opportunities to use complementary information from each to inform factors driving

313   aerosol pH. ISORROPIA's assumption of an internally mixed aerosol distribution cannot be

314   applied to predict pH in this system (Fountoukis and Nenes, 2007). However, it does provide

315   insight into the likely presence of coarse mode particles with pH significantly higher than the

316   fine mode. Conversely, Na^+, Cl^- and NO_3^- are not direct inputs into the pH calculation using

317   NH_3 partitioning, though they are used to compute aerosol liquid water, which is an input in the

318   pH calculation (Zheng et al., 2020). These NVCs have been shown to have sometimes

319   significant effects on the ratios of ammonium-sulfate, which could lead to inconsistencies in the

320   calculation of aerosol pH when considered in the ALWC calculation only (Guo et al. 2015).

321   NH_4^+ resides predominantly in the fine mode (Seinfeld and Pandis, 2016), so the partitioning

322   approach is unlikely to capture the acidity of the coarse mode or fine-mode particles in the tail of

323   the distribution of primary emissions that may be externally mixed with secondary particles, such

324   as dust or sea salt. This may lead to underestimates of NVC effects on aerosol pH using the

325   partitioning approach. The combined information from both methods suggests that aerosols

326   sampled at HMI during the NaCl event were characterized by a strong size-dependent pH

327   gradient, with fine-mode particles more acidic (pH ~2) than the coarse mode (pH up to 4.5).

328   Estimates of pH derived from size-segregated aerosol composition measurements have observed

329   the same phenomenon (Angle et al., 2021; Fang et al., 2017; Kakavas et al., 2021; Keene et al.,

330   2002).

331

332   **4 Conclusions**

333   There is growing recognition of the importance of aerosol pH affecting atmospheric

334   processes relevant to public health and ecosystems (Fang et al., 2017; Nenes et al., 2021).

335   Observations of spatial and temporal variations in pH are needed so that the factors that control

336   pH and contribute to variability in different environments can be fully understood. This study is

337   unique as it represents the first characterization of aerosol pH at a land-water transition site near

338   a large urban area. Baltimore, MD, is impacted by regional agricultural emissions and by

339   industrial point-source emissions of NH_3. The companion paper examines the sources of

340   episodic NH_3 events and the associated effects on aerosol composition (Balasus et al., 2021).

341   Although average and peak NH_3 concentrations during this study were significantly higher than a

342   nearby inland site, the effects on aerosol pH appear relatively insignificant, as pH during the

343   peak events was only ~0.1 pH unit higher than non-event periods. This finding is consistent with

344   studies at other locations that show aerosol pH is often insensitive to Tot-NH_3 and to the aerosol

345   NH_4:SO_4 ratio (Weber et al., 2016; Zheng et al., 2020; Tao and Murphy, 2019).

346   The unique characteristics of the OWLETS-2 study and measurement locations also

347   offered insight into the composition and meteorological influences on aerosol pH. In the

348   companion paper, the composition effects were shown to be muted in comparison to the

349   meteorological effects (Balasus et al., 2021). It was shown that the unique diurnal profiles,

350   particularly in ALW (which did not correlate with RH) and ε_{NH3} (which did not correlate with T)

351   resulted in meteorological factors, notably temperature, having the most important influence on

352   aerosol pH. Across the full temperature range of the study, the observed pH sensitivity to

353   temperature was -0.047 K^{-1}, with increases in sensitivity up to -0.085 K^{-1} when the temperature

354   was > 293 K. The sensitivity of aerosol pH shown here is in good agreement with previous

355   studies in the Baltimore region and beyond, *e.g.* Toronto (Tao and Murphy, 2019; Battaglia et al.

356   2017). Conversely, aerosol pH was not strongly affected by ALWC during the OWLETS-2

357   study, except when ALWC was below 1 $\mu g\ m^{-3}$, in contrast to the results of Zheng et al. (2020).

358   These results of Zheng et al. (2020) in identifying ALW as the most important factor driving

359   aerosol pH variability were derived from the results of studies in multiple locations, including

360   bulk aqueous solution. However, the analysis suggests that the factors that drive aerosol pH

361   variability may exhibit important site-to-site differences that must be considered before

362   generalizations are applied.

363   A case study of the NVC effect on aerosol pH had significantly different outcomes

364   depending on the method for calculating pH. ISORROPIA predicted a pH increase of ~ 1.4 pH

365   units during an event with primary aerosol emissions from the Chesapeake Bay, while the pH

366   calculation using NH_3 partitioning predicted a much less significant effect (~0.1 pH unit). This

367   difference is attributed to the likely presence of externally mixed particles during the events,

368   which may include primary marine emissions elevated in NVCs. Bougiatioti et al. (2016)

369   evaluated aerosol pH at a remote site in the Mediterranean, where samples with a marine origin

370   demonstrated vastly different pH between fine (avg. pH = 0.4) and coarse mode (average pH =

371   7.3) particles. Similarly, Keene et al. (2002) demonstrated the effect of marine aerosol size

372   distribution on aerosol pH, with fine mode particles predicted to reside in the range of 1-2, with

373 super-μm particles to reside in the range of 3-4, consistent with the current results. Hence, a

374 limitation of this study is the lack of size-resolved aerosol composition measurements. This

375 study underscores the need to evaluate assumptions of internally mixed aerosols when applying

376 pH calculations, which may be a critical factor in overestimating the effects of NVCs on pH.

377 Models with size-resolved aerosol composition may be required to capture this effect across

378 scales in future studies (Kakavas et al., 2021).

379

380 **Data Availability**

381 Data are available at https://www-air.larc.nasa.gov/cgi-bin/ArcView/owlets.2018.

382

383 **Supplement**

384 The supplement related to this article is available online at:

385

393

394 **Author Contributions**

395   CH, AC, and RD conceived the analysis and study participation. MB, NB, and KB collected and

396   analyzed the PILS-IC and NH_3 data. NB, MB, and CH conducted the thermodynamic modeling

397   analyses. VC and AC provided analytical input and interpretation. NB, CH, KB, and MB wrote

398   the manuscript. All authors provided feedback and revisions to the manuscript.

399

400   **Competing Interests**

401   The authors declare they have no conflict of interest.

402   **Figures**

403
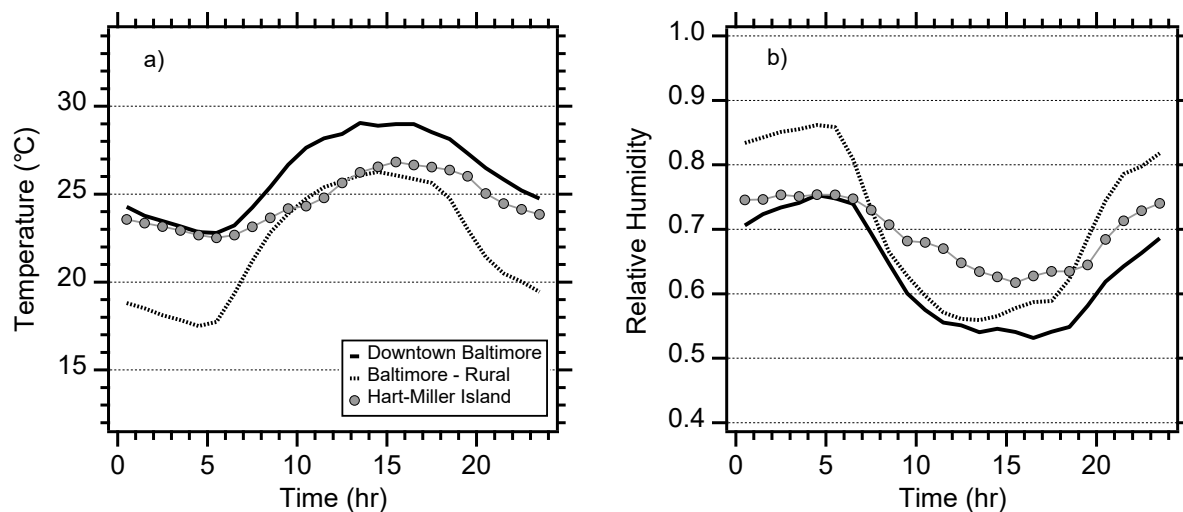
404

405   **Figure 1:** Diurnal profiles of (a) temperature and (b) relative humidity at three sites during the

406   OWLETS-2 study. Hart-Miller Island (HMI) is a land-water transition site and was the location

407   of aerosol composition and gas-phase measurements during the campaign. Temperatures at HMI

408   resembled the downtown location during the night but showed characteristics of the rural site

409   during the day. RH at HMI was between the urban and rural sites at night but was elevated

410   during the daytime due to the Chesapeake Bay.

411
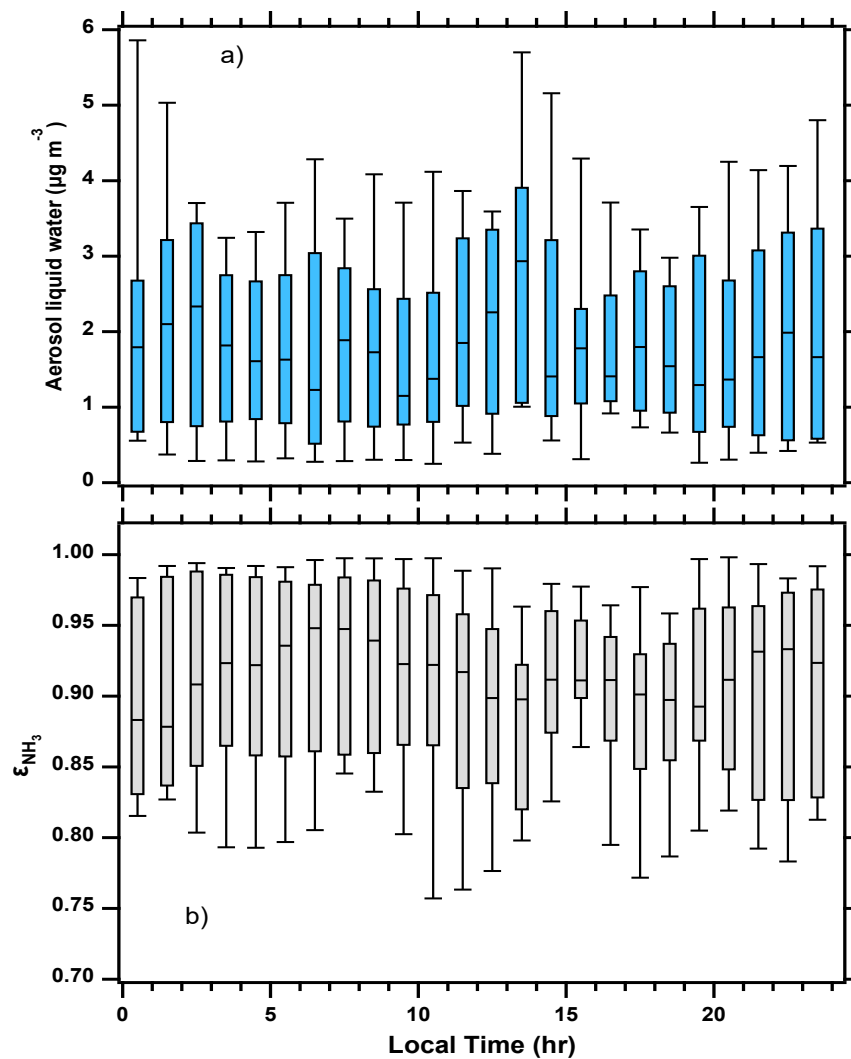
Figure 2: Box plots of (a) aerosol liquid water and (b) ε_{NH3} (ε_{NH3} = NH₃(g)/(NH₃(g) + NH₄⁺(aq)))

during the OWLETS-2 study. The statistics shown are the median, quartiles, 10th and 90th
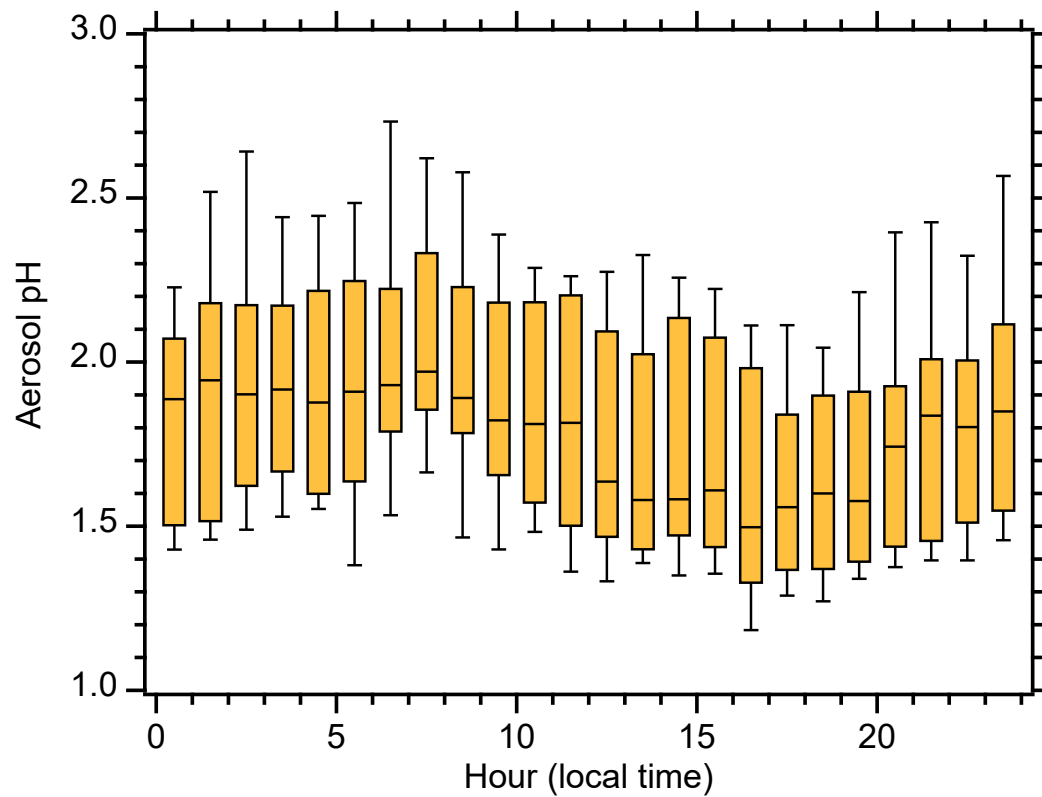
percentiles.

415

416   **Figure 3:** Box plot of the aerosol pH diurnal profile calculated using the method of Zheng et al.

417   (2020) at Hart-Miller Island during OWLETS-2. The statistics shown are the median, quartiles,

418   10th and 90th percentiles.

419
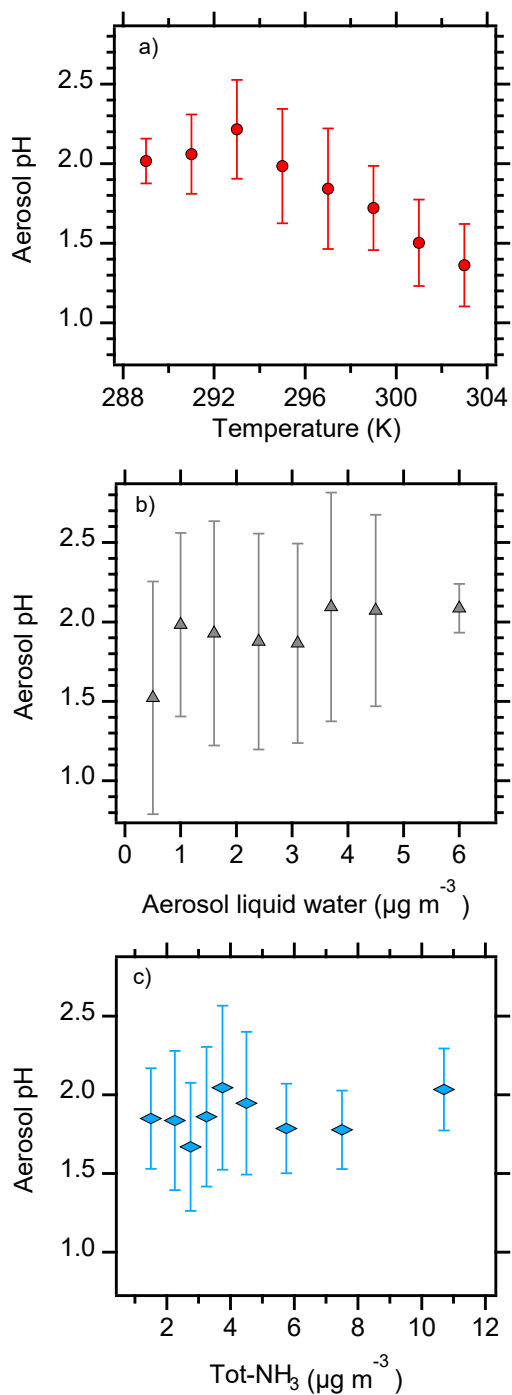
Figure 4: Relationship between aerosol pH and (a) temperature, (b) aerosol liquid water, and (c)

total NH$_3$ (Tot-NH$_3$ = NH$_3$ + NH$_4^+$). Symbols represent mean values while error bars represent

standard deviations.

423
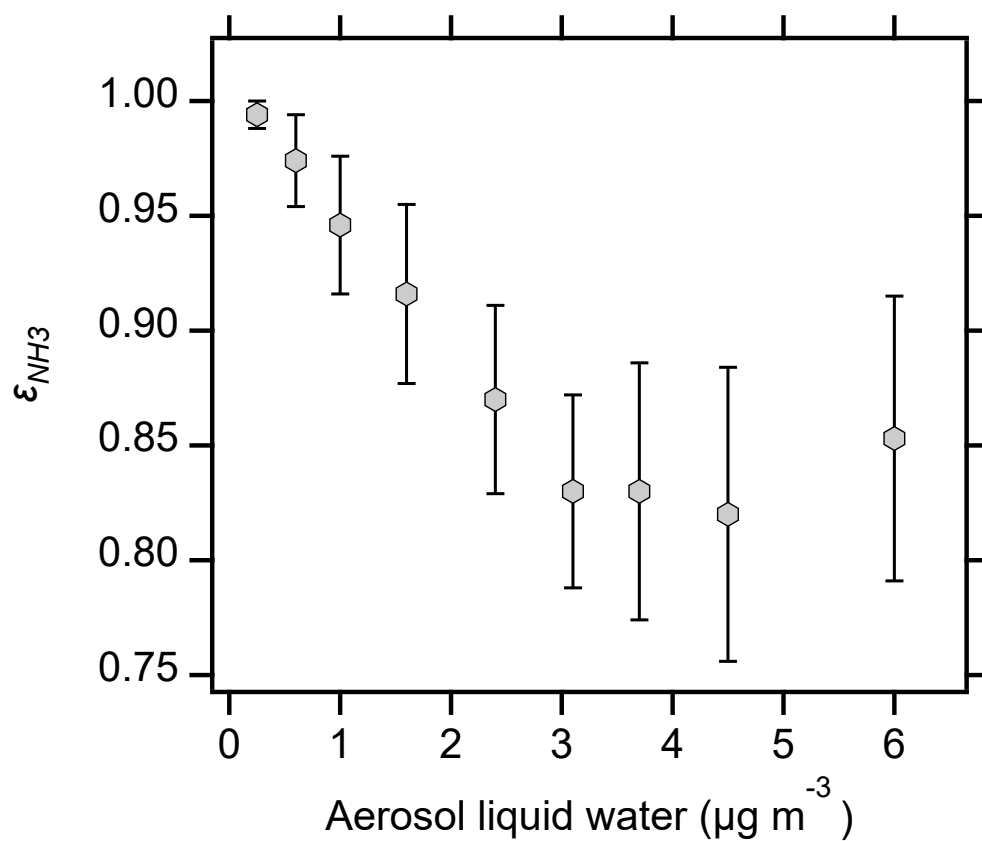
Figure 5: Relationship between NH_3 partitioning ($\varepsilon_{NH3} = NH_3/(NH_3 + NH_4^+)$) and aerosol liquid

water. Symbols represent mean values while error bars represent standard deviations.

426
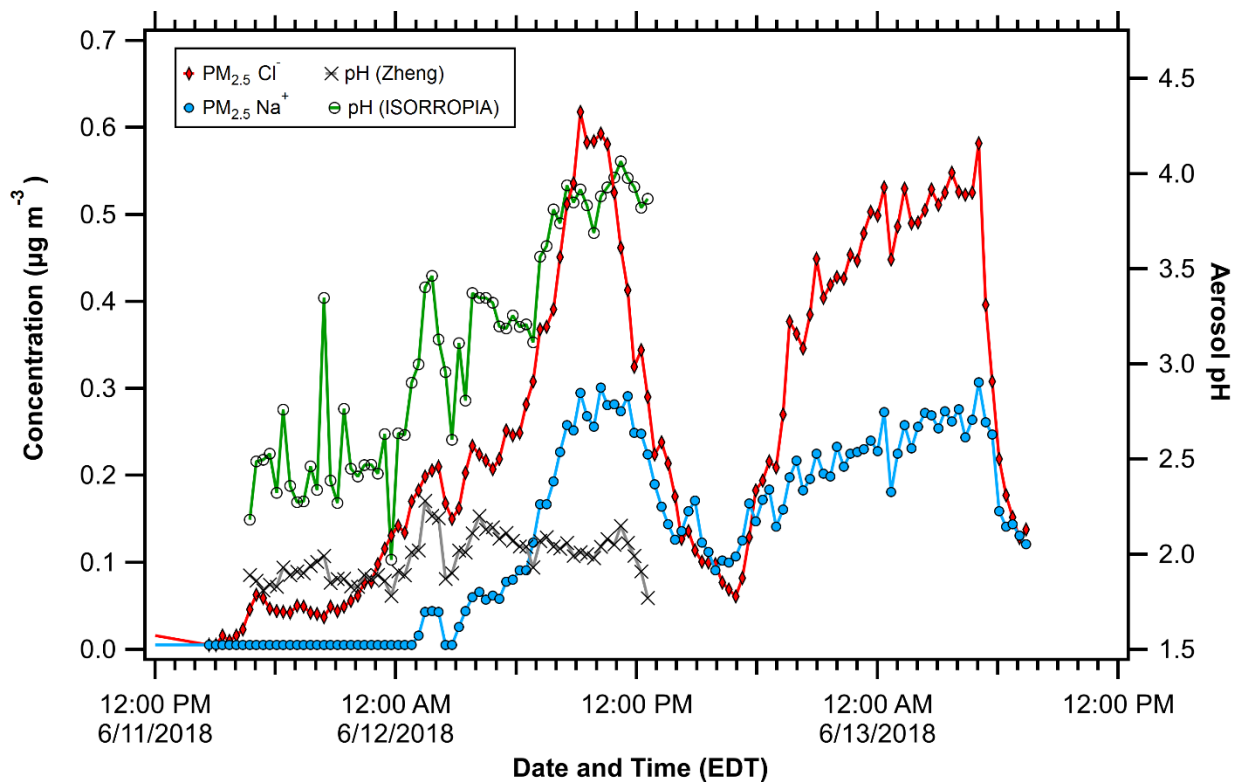
Figure 6: Concentrations of PM$_{2.5}$ Na$^+$ and Cl$^-$ during a period with primary Chesapeake Bay emissions. Aerosol pH calculated by NH$_3$ partitioning (Zheng et al. method) and ISORROPIA show different behaviors, suggesting the aerosol distribution was externally mixed during this time.
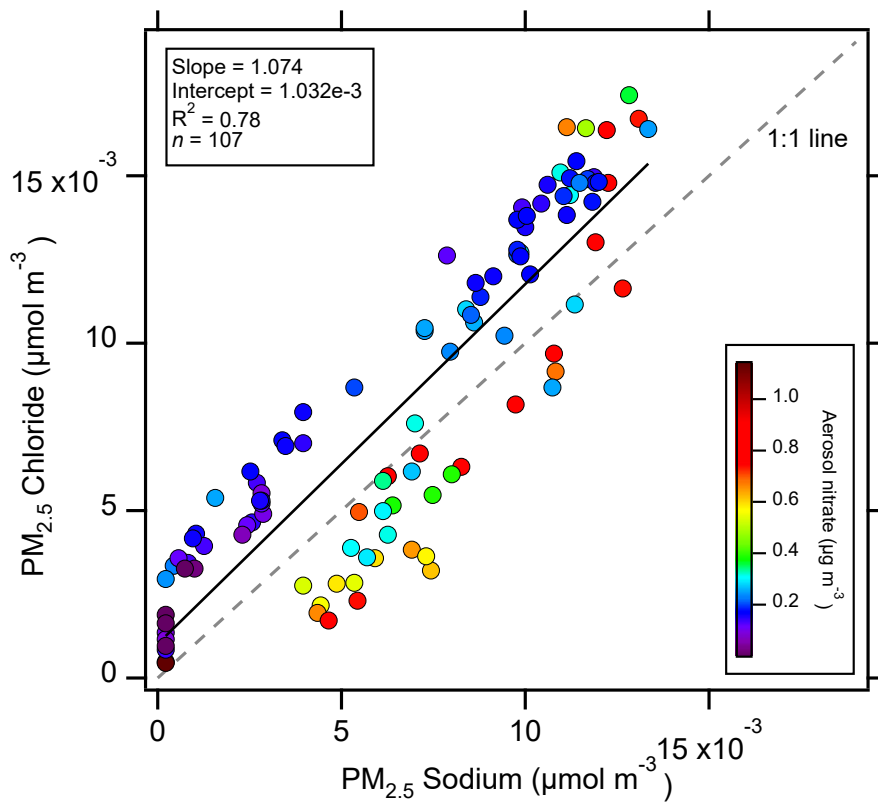
Figure 7: Correlation between $PM_{2.5}$ Na^+ and Cl^- during the event shown in Figure 6. Lower chloride:sodium ratios were observed at higher NO_3^- concentrations, suggesting HNO_3 uptake displaced HCl.

References

Angle, K. J., Crocker, D. R., Simpson, R. M. C., Mayer, K. J., Garofalo, L. A., Moore, A. N., Garcia, S. L. M., Or, V. W., Srinivasan, S., Farhan, M., Sauer, J. S., Lee, C., Pothier, M. A., Farmer, D. K., Martz, T. R., Bertram, T. H., Cappa, C. D., Prather, K. A., and Grassian, V. H. (2021). Acidity across the interface from the ocean surface to sea spray aerosol. *Proceedings of the National Academy of Sciences of the United States of America*, *118*(2), Article e2018397118. https://doi.org/10.1073/pnas.2018397118

Balasus, N., Battaglia, M. A., Ball, K., Caicedo, V., Delgado, R., Carlton, A.G., and Hennigan, C.J. (2021). Urban aerosol chemistry at a land-water transition site during summer - part 1: impact of agricultural and industrial ammonia emissions. *Atmos. Chem. Phys. Discussions. In review.*

Battaglia Jr, M. A., Weber, R. J., Nenes, A., and Hennigan, C. J. (2019). Effects of water-soluble organic carbon on aerosol pH. *Atmos. Chem. Phys.*, *19*(23), 14607-14620. https://doi.org/10.5194/acp-19-14607-2019

Battaglia, M. A., Douglas, S., and Hennigan, C. J. (2017). Effect of the Urban Heat Island on Aerosol pH. *Environ. Sci. Technol.*, *51*(22), 13095-13103. https://doi.org/10.1021/acs.est.7b02786

Bougiatioti, A., Nikolaou, P., Stavroulas, I., Kouvarakis, G., Weber, R., Nenes, A., Kanakidou, M., and Mihalopoulos, N. (2016). Particle water and pH in the eastern Mediterranean: source variability and implications for nutrient availability. *Atmos. Chem. Phys.*, *16*(7), 4579-4591. https://doi.org/10.5194/acp-16-4579-2016

Brimblecombe, P., and Clegg, S. L. (1988). The Solubility and Behavior of Acid Gases in the Marine Aerosol. *Journal of Atmospheric Chemistry*, *7*(1), 1-18. https://doi.org/10.1007/bf00048251

Carlton, A. M. G., Pye, H. O. T., Baker, K. R., and Hennigan, C. J. (2018). Additional benefits of federal air quality rules: model estimates of controllable biogenic secondary organic aerosol. *Environmental Science and Technology*. https://doi.org/10.1021/acs.est.8b01869

El-Sayed, M. M. H., Amenumey, D., and Hennigan, C. J. (2016). Drying-Induced Evaporation of Secondary Organic Aerosol during Summer. *Environmental Science and Technology*, *50*(7), 3626-3633. https://doi.org/10.1021/acs.est.5b06002

Fang, T., Guo, H. Y., Zeng, L. H., Verma, V., Nenes, A., and Weber, R. J. (2017). Highly Acidic Ambient Particles, Soluble Metals, and Oxidative Potential: A Link between Sulfate and Aerosol Toxicity. *Environmental Science and Technology*, *51*(5), 2611-2620. https://doi.org/10.1021/acs.est.6b06151

Feng, L., Shen, H., Zhu, Y., Gao, H., and Yao, X. (2017). Insight into Generation and Evolution of Sea-Salt Aerosols from Field Measurements in Diversified Marine and Coastal Atmospheres. *Scientific Reports*, *7*, Article 41260. https://doi.org/10.1038/srep41260

Fountoukis, C., and Nenes, A. (2007). ISORROPIA II: a computationally efficient thermodynamic equilibrium model for K^+-Ca^{2+}-Mg^{2+}-NH_4^+-Na^+-SO_4^{2-}-NO_3^--Cl^--H_2O aerosols. *Atmos. Chem. Phys.*, *7*(17), 4639-4659. https://doi.org/10.5194/acp-7-4639-2007

Guo, H., Liu, J., Froyd, K. D., Roberts, J. M., Veres, P. R., Hayes, P. L., Jimenez, J. L., Nenes, A., and Weber, R. J. (2017). Fine particle pH and gas–particle phase partitioning of inorganic species in

476   Pasadena, California, during the 2010 CalNex campaign. *Atmos. Chem. Phys.*, *17*(9), 5703-5719.
477   https://doi.org/10.5194/acp-17-5703-2017

478 Guo, H., Nenes, A., and Weber, R. J. (2018). The underappreciated role of nonvolatile cations in aerosol
479   ammonium-sulfate molar ratios. *Atmos. Chem. Phys.*, *18*(23), 17307-17323.
480   https://doi.org/10.5194/acp-18-17307-2018

481 Guo, H., Xu, L., Bougiatioti, A., Cerully, K. M., Capps, S. L., Hite, J. R., Carlton, A. G., Lee, S. H.,
482   Bergin, M. H., Ng, N. L., Nenes, A., and Weber, R. J. (2015). Fine-particle water and pH in the
483   southeastern United States. *Atmos. Chem. Phys.*, *15*(9), 5211-5228. https://doi.org/10.5194/acp-
484   15-5211-2015

485 He, H., Stehr, J. W., Hains, J. C., Krask, D. J., Doddridge, B. G., Vinnikov, K. Y., Canty, T. P., Hosley,
486   K. M., Salawitch, R. J., Worden, H. M., and Dickerson, R. R. (2013). Trends in emissions and
487   concentrations of air pollutants in the lower troposphere in the Baltimore/Washington airshed
488   from 1997 to 2011. *Atmospheric Chemistry and Physics*, *13*(15), 7859-7874.
489   https://doi.org/10.5194/acp-13-7859-2013

490 Hennigan, C. J., Izumi, J., Sullivan, A. P., Weber, R. J., and Nenes, A. (2015). A critical evaluation of
491   proxy methods used to estimate the acidity of atmospheric particles. *Atmos. Chem. Phys.*, *15*(5),
492   2775-2790. https://doi.org/10.5194/acp-15-2775-2015

493 Kakavas, S., Patoulias, D., Zakoura, M., Nenes, A., and Pandis, S. N. (2021). Size-resolved aerosol pH
494   over Europe during summer. *Atmos. Chem. Phys.*, *21*(2), 799-811. https://doi.org/10.5194/acp-21-
495   799-2021

496 Kanakidou, M., Myriokefalitakis, S., Daskalakis, N., Fanourgakis, G., Nenes, A., Baker, A. R., Tsigaridis,
497   K., and Mihalopoulos, N. (2016). Past, Present, and Future Atmospheric Nitrogen Deposition. *J.*
498   *Atmos. Sci.*, *73*(5), 2039-2047. https://doi.org/10.1175/jas-d-15-0278.1

499 Keene, W. C., Pszenny, A. A. P., Maben, J. R., and Sander, R. (2002). Variation of marine aerosol acidity
500   with particle size. *Geophysical Research Letters*, *29*(7), Article 1101.
501   https://doi.org/10.1029/2001gl013881

502 Keene, W. C., Pszenny, A. A. P., Maben, J. R., Stevenson, E., and Wall, A. (2004). Closure evaluation of
503   size-resolved aerosol pH in the New England coastal atmosphere during summer. *J. Geophys.*
504   *Res.-Atmos.*, *109*(D23), D23307, Article D23307. https://doi.org/10.1029/2004jd004801

505 Loughner, C. P., Tzortziou, M., Follette-Cook, M., Pickering, K. E., Goldberg, D., Satam, C.,
506   Weinheimer, A., Crawford, J. H., Knapp, D. J., Montzka, D. D., Diskin, G. S., and Dickerson, R.
507   R. (2014). Impact of Bay-Breeze Circulations on Surface Air Quality and Boundary Layer
508   Export. *Journal of Applied Meteorology and Climatology*, *53*(7), 1697-1713.
509   https://doi.org/10.1175/jamc-d-13-0323.1

510 Loughner, C. P., Tzortziou, M., Shroder, S., and Pickering, K. E. (2016). Enhanced dry deposition of
511   nitrogen pollution near coastlines: A case study covering the Chesapeake Bay estuary and
512   Atlantic Ocean coastline. *Journal of Geophysical Research-Atmospheres*, *121*(23), 14221-14238.
513   https://doi.org/10.1002/2016jd025571

514   Nenes, A., Pandis, S. N., Kanakidou, M., Russell, A. G., Song, S., Vasilakos, P., and Weber, R. J. (2021).
515   Aerosol acidity and liquid water content regulate the dry deposition of inorganic reactive
516   nitrogen. *Atmos. Chem. Phys.*, *21*(8), 6023-6033. https://doi.org/10.5194/acp-21-6023-2021

517   Nenes, A., Pandis, S. N., Weber, R. J., and Russell, A. (2020). Aerosol pH and liquid water content
518   determine when particulate matter is sensitive to ammonia and nitrate availability. *Atmos. Chem.
519   Phys.*, *20*(5), 3249-3258. https://doi.org/10.5194/acp-20-3249-2020

520   Norman, M., Spirig, C., Wolff, V., Trebs, I., Flechard, C., Wisthaler, A., Schnitzhofer, R., Hansel, A., and
521   Neftel, A. (2009). Intercomparison of ammonia measurement techniques at an intensively
522   managed grassland site (Oensingen, Switzerland). *Atmospheric Chemistry and Physics*, *9*(8),
523   2635-2645.

524   O'Dowd, C. D., and De Leeuw, G. (2007). Marine aerosol production: a review of the current knowledge.
525   *Philosophical Transactions of the Royal Society a-Mathematical Physical and Engineering
526   Sciences*, *365*(1856), 1753-1774. https://doi.org/10.1098/rsta.2007.2043

527   Phillips, S. M., Bellcross, A. D., and Smith, G. D. (2017). Light Absorption by Brown Carbon in the
528   Southeastern United States is pH-dependent. *Environmental Science and Technology*.
529   https://doi.org/10.1021/acs.est.7b01116

530   Pinder, R. W., Adams, P. J., Pandis, S. N., and Gilliland, A. B. (2006). Temporally resolved ammonia
531   emission inventories: Current estimates, evaluation tools, and measurement needs. *Journal of
532   Geophysical Research-Atmospheres*, *111*(D16), Article D16310.
533   https://doi.org/10.1029/2005jd006603

534   Pritchard, D. W. (1952). Salinity Distribution and Circulation in the Chesapeake Bay Estuarine System.
535   *Journal of Marine Research*, *11*(2), 106-123.

536   Pszenny, A. A. P., Moldanov, J., Keene, W. C., Sander, R., Maben, J. R., Martinez, M., Crutzen, P. J.,
537   Perner, D., and Prinn, R. G. (2004). Halogen cycling and aerosol pH in the Hawaiian marine
538   boundary layer. *Atmospheric Chemistry and Physics*, *4*, 147-168. https://doi.org/10.5194/acp-4-
539   147-2004

540   Pye, H. O. T., Nenes, A., Alexander, B., Ault, A. P., Barth, M. C., Clegg, S. L., Collett Jr, J. L., Fahey, K.
541   M., Hennigan, C. J., Herrmann, H., Kanakidou, M., Kelly, J. T., Ku, I. T., McNeill, V. F.,
542   Riemer, N., Schaefer, T., Shi, G., Tilgner, A., Walker, J. T., Wang, T., Weber, R., Xing, J.,
543   Zaveri, R. A., and Zuend, A. (2020). The acidity of atmospheric particles and clouds. *Atmos.
544   Chem. Phys.*, *20*(8), 4809-4888. https://doi.org/10.5194/acp-20-4809-2020

545   Pye, H. O. T., Zuend, A., Fry, J. L., Isaacman-VanWertz, G., Capps, S. L., Appel, K. W., Foroutan, H.,
546   Xu, L., Ng, N. L., and Goldstein, A. H. (2018). Coupling of organic and inorganic aerosol
547   systems and the effect on gas–particle partitioning in the southeastern US. *Atmos. Chem. Phys.*,
548   *18*(1), 357-370. https://doi.org/10.5194/acp-18-357-2018

549   Seinfeld, J. H., and Pandis, S. N. (2016). *Atmospheric chemistry and physics: from air pollution to
550   climate change* (3 ed.). John Wiley and Sons.

551   Tao, Y. (2020). *Identification of Major Factors Influencing Aerosol pH and the Quantitative Relationship
552   between pH and Ammonia Gas/Particle Partitioning* [Doctoral thesis, University of Toronto].
553   University of Toronto TSpace. https://hdl.handle.net/1807/103788

554 Tao, Y., and Murphy, J. G. (2019). The sensitivity of PM2.5 acidity to meteorological parameters and
555   chemical composition changes: 10-year records from six Canadian monitoring sites. *Atmos.*
556   *Chem. Phys.*, *19*(14), 9309-9320. https://doi.org/10.5194/acp-19-9309-2019

557 Valerino, M. J., Johnson, J. J., Izumi, J., Orozco, D., Hoff, R. M., Delgado, R., and Hennigan, C. J.
558   (2017). Sources and composition of PM2.5 in the Colorado Front Range during the DISCOVER-
559   AQ study. *Journal of Geophysical Research-Atmospheres*, *122*(1), 566-582.
560   https://doi.org/10.1002/2016jd025830

561 Vasilakos, P., Russell, A., Weber, R., and Nenes, A. (2018). Understanding nitrate formation in a world
562   with less sulfate. *Atmos. Chem. Phys.*, *18*(17), 12765-12775. https://doi.org/10.5194/acp-18-
563   12765-2018

564 Weber, R. J., Guo, H., Russell, A. G., and Nenes, A. (2016). High aerosol acidity despite declining
565   atmospheric sulfate concentrations over the past 15 years [Letter]. *Nature Geoscience*, *9*(4), 282-
566   285. https://doi.org/10.1038/ngeo2665

567 Zheng, G., Su, H., Wang, S., Andreae, M. O., Pöschl, U., and Cheng, Y. (2020). Multiphase buffer theory
568   explains contrasts in atmospheric aerosol acidity. *Science*, *369*(6509), 1374.
569   https://doi.org/10.1126/science.aba3719